Acta Oceanol. Sin., 2020, Vol. 39, No. 10, P. 70–80
https://doi.org/10.1007/s13131-020-1661-6
http://www.hyxb.org.cn
E-mail: hyxbe@263.net

Calcareous nannofossil changes in the Early Oligocene linked to nutrient and atmospheric CO_2

Ruigang Ma[1], Haizhang Yang[2], Xiaobo Jin[1], Zhao Zhao[2], Gongcheng Zhang[2], Chuanlian Liu[1]*
[1] State Key Laboratory of Marine Geology, Tongji University, Shanghai 200092, China
[2] CNOOC Research Institute Co., Ltd., Beijing 100027, China

Received 18 March 2020; accepted 3 June 2020

Abstract

Rapid changes on nutrient supply and CO_2 concentration that occurred in the northern South China Sea (SCS) during the Early Oligocene, provides an ideal natural laboratory, allowing us to peer into the coccolithophores' physiology in the geological records. In this study, we established a new nannofossil assemblage index, termed as E^* ratio, which is calculated by the relative abundance of eutrophic taxa and meso-oligotrophic taxa ($E^* = \frac{e}{e+c} \times 100$, where e is eutrophic taxa, and c is meso-oligotrophic taxa). Eutrophic taxa include small *Reticulofenestra*, *Reticulofenestra lockeri* group, *Reticulofenestra bisecta* group and *Coccolithus pelagicus* group, while meso-oligotrophic taxa include *Cyclicargolithus* spp. The E^* ratio is well correlated with nutrient proxy during the Early Oligocene, while with different covarying patterns under the higher and lower CO_2 condition. By comparing the assemblage changes to the published data, we suggest that coccolithophores may change the way they use carbon source and nutrient with the decline of CO_2. Furthermore, this implies a possible initiation of the carbon concentrating mechanism.

Key words: coccolithophore, assemblage change, weathering intensity, carbon concentrating mechanism, northern South China Sea

Citation: Ma Ruigang, Yang Haizhang, Jin Xiaobo, Zhao Zhao, Zhang Gongcheng, Liu Chuanlian. 2020. Calcareous nannofossil changes in the Early Oligocene linked to nutrient and atmospheric CO_2. Acta Oceanologica Sinica, 39(10): 70–80, doi: 10.1007/s13131-020-1661-6

1 Introduction

Coccolithophores (marine calcifying phytoplankton) comprise up to 20% of the phytoplankton carbon pool in open ocean regions (Poulton et al., 2007). This unique phytoplankton plays an important role in the oceanic carbon cycle due to their physiological processes. The calcification (release CO_2) and photosynthesis (absorb CO_2) contribute to the marine carbonate-counter pump and biological pump, respectively. Studies on modern species have revealed that coccolithophores have a relatively inefficient carbon concentrating mechanism (CCM), thus can be carbon limited compared to other phytoplankton for photosynthesis under low CO_2 conditions (Bach et al., 2013; Reinfelder, 2011; Riebesell, 2004; Rost et al., 2003). Besides, the growth of the coccolithophores could be influenced by many factors. For example, nitrate controls the cell growth, affecting the size of the cell, while phosphorous controls the mitosis, affecting the abundance of the cells (Müller et al., 2008). Light intensity influences the rate of the cell photosynthesis. The temperature has great limitations on the activity of enzymes, which concern with almost every physiological process within the cell (Krumhardt et al., 2017). It is widely believed that different limitations will lead to different adaptive strategies. However, existing studies tended to minimize the complexity and flexibility of the nannoplankton responses to paleoceanographic changes.

As the most successful and yet enigmatic organism in the modern ocean, the coccolithophores have the capability of adjusting their living strategy to adapt to the environmental changes (Aubry, 2007, 2009), for example, the strategy of utilizing the carbon resources. A coccolith isotopic record from Early Miocene to Pleistocene suggested that aqueous CO_2 concentration of 16–19 μmol/L is the threshold of the coccolithophores' CCM (Bolton and Stoll, 2013). During the Eocene-Oligocene Boundary, Earth's climate has undergone a significant cooling and continental ice-sheet expanding, as revealed by the benthic $\delta^{18}O$ (Zachos et al., 2001; Cramer et al., 2009, 2011). Atmospheric CO_2 declined around 500×10^{-6} (volume fraction) during the Early Oligocene (Pagani et al., 2005, 2011; Zhang et al., 2013). Although there are some coccolithophores assemblage records of Oligocene (Bown et al., 2004), the study of the driving mechanisms for this physiological change are still insufficient (Plancq et al., 2013; Henderiks and Pagani, 2008; Müller et al., 2017).

The northern South China Sea (SCS) provides a relatively stable and semi-enclosed environment after its spreading since the earliest Oligocene (Li et al., 2006; Zhang et al., 2015; Jian et al., 2019; Ma et al., 2019). Yet, variations of terrestrial input caused dramatic changes in the nutrient condition during this period. Pollen analysis from ODP Site 1148 revealed that a relatively arid and cool climate was developed since 32 Ma in the nearby continent (Wu et al., 2003). In this study, we provide coccolith records and bulk sediment elemental ratios data covering 34–27 Ma from sites in the northern SCS.

Foundation item: The National Science and Technology Major Project of the Ministry of Science and Technology of China under contract No. 2016ZX05026007-03; the National Natural Science Foundation of China under contract Nos 41876046 and 41930536.
*Corresponding author, E-mail: liucl@tongji.edu.cn

2 Materials and methods

2.1 *Study sites and samples*

We combined records from three sites in the northern SCS to lower the possible bias caused by the effect of redeposition on the calcareous nannofossils (Fig. 1). Sites U1501 and U1505 were retrieved during the International Ocean Discovery Program (IODP) cruise Exp. 367/368. Site U1501 (18°53′N, 115°46′E) lies on a broad basement high in the lower slope of the northern SCS at a water depth of 2 845.8 m, which is above the temporal CCD at ~3 500 m (Wang, 1999). For the first time in the region, relatively continuous sediment cores with well-preserved Early Oligocene calcareous nannofossils were recovered from this site. Sixty-seven samples were collected every 90 cm from 373.18 m to 303.95 m (CSF-A) in Hole U1501 C.

Site U1505 (18°55.0′N, 115°51.5′E) is located at a water depth of 2 916.6 m on a broad regional basement high. It was an alternate to Site U1501. Both Sites U1505 and U1501 are located on the same structural high with similar water depths and are 10.5 km apart. These two sites are believed to have similar tectonic background. Site U1505, however, have wider interval that considered as the slum zone caused by tectonic activity (Jian et al., 2019). We collected 38 samples from Hole U1505 C in the lower part of the Lower Oligocene (417.66–444.55 m), spacing varied from 40 cm to 90 cm.

Borehole LW2 (19°30′N, 115°40′E) was retrieved in the western Liwan Sub-sag, Baiyun Sag, Zhujiang (Pearl) River Mouth Basin. This industrial borehole located at around 1 800 m water depth, above the temporal CCD, which guarantees great preservation of calcareous fossils. Fifty-five samples were collected from 3 266 m to 3 841 m (total depth) from this site, spacing around 10 m.

2.2 *Calcareous nannofossil*

The samples were prepared following the technique of Koch and Young (2007) modified by Bordiga et al. (2015), allowing absolute quantification of nannofossil abundances per gram of sediment. The taxonomic nomenclature described in Nannotax 3 (Young et al., 2018) was followed. Each sample was prepared by weighing 0.2–0.5 g of dried bulk sediment and diluting with 100–250 mL of buffered water. Then 100–500 μL well-mixed suspension was placed on a cover slip with a high-precision pipette and dried on a hotplate at 35°C. The weight of sediment, volume of dilution and the suspension on the cover slip were adjusted according to the abundance of the nannofossil in each sample. Settled slides were examined using Zeiss Scope A1 microscope under a cross polarizer and a magnification of 1 250×. On each slide, more than 300 calcareous nannofossils were counted. For each sample, the absolute (ind./g) and relative (%) species abundances are both calculated following Bordiga et al. (2015).

Coccolith fluxes were calculated by using the following formula:

$$F = XR_aD, \tag{1}$$

where F is the coccolith flux (ind./(mm^2·ka)), X is the absolute abundance (ind./g) of total nannofossil, R_a is the accumulation rates (mm/ka) that calculated by nannofossil controlling bioevents, and D is the bulk dry-density (g/mm^3) from Larsen et al. (2018).

The E^* ratio as an assemblage index is for the first time developed in this study:

$$E^* = \frac{e}{e+c} \times 100, \tag{2}$$

where e represents the combined relative abundance of eutrophic taxa (see Section 3.1), and c is the relative abundance of *Cycli-*

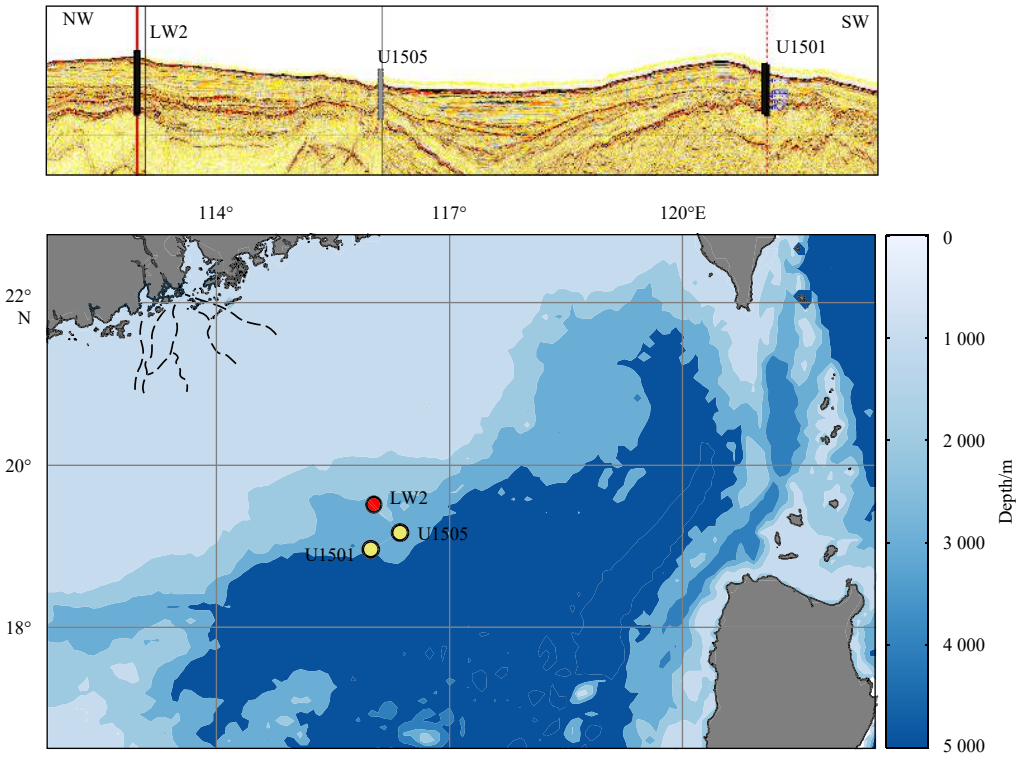

Fig. 1. Location of the IODP Sites U1501, U1505 and the Borehole LW2. Site U1505 is only approximately located on the seismic profile.

cargolithus spp. The Oligocene Nannoplankton community is featured by the great and very common appearance of the *Cyclicargolithus*. The *Cyclicargolithus floridanus* is a sub-group of the circular *Reticulofenestra* with a narrower central area, which is common in many Paleogene marine sections yet its ecological preference remains ambiguous. Some authors considered *Cy. floridanus* as a warm (Aubry, 1992) or eutrophic taxon (Aubry, 1992; Dunkley Jones et al., 2008; Auer et al., 2014; Fioroni et al., 2015), while others claimed it as an indicator of decreased nutrient supply or lower ocean productivity (Bordiga et al., 2015; Toffanin et al., 2011; Ma et al., 2019). In this study, we refer it as a non-nutrient indictive taxa, based on their cosmopolitan appearance in the ocean and through our study interval. Taxa that believed to be sensitive and indicative to nutrient condition of the sea water are as follows: *C. pelagicus* (Cachão and Moita, 2000; Fernando et al., 2007; Jin et al., 2016; Tangunan et al., 2018), *R. lockeri* group (Newsam et al., 2017; Persico and Villa, 2004; Villa et al., 2008), *R. bisecta* group (Persico and Villa, 2004; Villa et al., 2008) and small *Reticulofenestra* (Flores et al., 1995; Henderiks and Pagani, 2008; Jatiningrum and Sato, 2017). This E^* ratio index is a good indicator of the community's demand for nutrients in seawater.

2.3 *Bulk sediment elemental analysis*

A total of 44 samples from 379.75 m to 304.56 m (~27–34 Ma) of Site U1501 were collected for geochemical analyses. Bulk sediments were first washed with deionized distilled water, dried at 50°C for 48 h and then hand crushed in an agate mortar. Approximately 3 g of dry samples were heated to 600°C for 2 h in order to remove organic matter and interlayer water. Next, the samples were digested in a HF-HNO_3 mixture, and major and trace elements were measured using ICP-AES and ICP-MS, respectively. Three certified materials (i.e., GSR-5, GSR-6, and GSD-9; provided by the Institute of Geophysical and Geochemical Exploration, China) were repeatedly analyzed as unknown samples to assess the precision and accuracy of the measurements. The external precision was usually better than 5% and concentrations obtained were in agreement with the recommended data of these reference materials. Analyses were carried out at the State Key Laboratory of Marine Geology, Tongji University.

Although many elemental proxies often have a low merit when applied to paleoenvironmental interpretations in coastal and shallow sea areas (Tribovillard et al., 2006), some elements have been shown as reliable proxies of weathering intensity, among others. In examining the climate change since 32 Ma we consider the proxies applied to weathering and erosion studies in a tectonic timescale.

Ti/Al ratio is broadly used as an eolian flux proxy, a higher Ti/Al value indicates more eolian sediment and thus a relatively arid climate. However, as we observed the samples under scanning electron microscope, we did not find any eolian sandy sediment (angular morphology of quartz) in Site U1501 during the Early Oligocene. On the other hand, titanium is concentrated in heavy minerals (e.g., ilmenite, rutile and zirconium) and in coarser silt and sand fractions (Schmitz, 1987; Shimmield and Mowbray, 1991). We thus believe that the TiO_2/Al_2O_3 ratio in U1501 represents the paleo-stream energy in this study.

Relative changes in Al and K at this site reflect the preferential enrichment of kaolinite (low K/Al) in warm/humid period and the better survival of feldspar (high K/Al) during drier periods (Clift et al., 2014). We used phosphorus (calculated from P_2O_5) as a nutrient proxy because: (1) PO_4 is the only source of phosphorus for phytoplankton in Earth system models (in contrast to nitrogen, which can be taken up by phytoplankton as nitrate or ammonia); (2) PO_4 availability has been shown to affect coccolithophore's calcification (Feng et al., 2017; Müller et al., 2008; Perrin et al., 2016); and (3) continental margins and marginal sediments, as the study sites of this paper, play a significant role in the cycling of phosphorus, with about 50% of total P input to the ocean deposited in marginal sediments (Filippelli, 2002).

In sea water, redox-sensitive Mn is mainly present as Mn^{2+}, which under oxic conditions precipitates as Mn oxyhydroxide. The Mn flux across the sediment–water interface is driven by reductive dissolution of reactive Mn oxyhydroxide (Neretin et al., 2003). In bulk sediment, and a higher Mn/Al value represents a relatively oxic condition, and a lower value of Mn/Al ratio usually indicates a sub-anoxic bottom water condition. Mn oxyhydroxides are ubiquitous components of oxidized pelagic clays, and such phases are unstable under the reducing conditions normally encountered at depth in marginal and some deep-sea environments, so they are only found in the sea-floor record in slowly accumulating deposits that have remained oxygenated since the deposits formed (Calvert and Pedersen, 2007). Mn/Al ratio as proxy of bottom water redox condition and ventilation is proved to be valid (e.g., McKay et al., 2015; Wu et al., 2016).

3 Results

3.1 *Calcareous nannofossil biostratigrphy*

The standard calcareous nannofossil NP-zonation (Martini, 1971) with calibrated ages for species datums (Raffi et al., 2016) were adopted in this study. Eight nannofossil bioevents ranging from Lower to Upper Oligocene are recognized in the three study sites (Table 1, Fig. 2). For Site U1501, the BO (base occurence) of common *Clausicoccus subdistichus* at 373.18 m (33.88 Ma) defines the closest bio-marker to Eocene-Oligocene Boundary (33.9 Ma), while the TO (top occurence) of *Coccolithus formosus* (32.92 Ma) at 356.99 m marks the boundary of NP21/NP22, and the TO of *Reticulofenestra umbilicus* (32.02 Ma) at 341.35 m the boundary of NP22/NP23. Furthermore, Zone NP 24 can be defined by the BO of Sphenolithus ciperonensis and TO of *Sphenolithus distentus* at 307.56 m and at 303.95 m, in the presence of *Sphenolithus predistentus*. The BO of *S. ciperoensis* (27.14 Ma) at 307.56 m approximates the Early/Late Oligocene boundary (Table 1).

Semblable but more tentative time controlls are recognized in U1505 and LW2. TO of *Sphenolithus predistentus* (26.93 Ma) was found at 407.45 m in U1505 and 3 285 m (total depth) in LW2. The TO of *Reticulofenestra umbilicus* (32.02 Ma, low latitude) was found in 424.92 m at U1505 and 3 773 m (total depth) in LW2. Because of the solubility effect, the TO of *Coccolithus formosus* (32.92 Ma) is difficult to be identified in U1505, and is only recognized in LW2 at the depth of 3 835 m. The Bc (base common occurence) of *Clausicoccus subdistichus* (33.88 Ma) (Raffi et al., 2016) in U1505 was found at the depth of 443.45 m. The TO of *Sphenolithus distentus* (26.84 Ma) and *Sphenolithus pseudoradians* (28.73 Ma) were found in LW2 at depth of 3 273 m and 3 395 m (total depth).

Age model was established based on controlling points recognized in each site with a liner interpolation in between (Fig. 2).

3.2 *Nannofossil assemblages and the E^* ratio*

For each sample, one nannofossil species (*Coccolithus pelagicus*), two species group (*Reticulofenestra lockeri* group and *Reticulofenestra bisecta* group) and three genra (*Cyclicargolithus, Sphenolithus* and *Helicosphaera*) are counted. *Reticulofenestra*

Table 1. Nannofossil bio-events and age model used in this study

Nannofossil bio-event	Site	Sample	Depth/m	Age/Ma
TO *Sphenolithus distentus*	U1501	45X-5-55/57	303.95	26.84
TO *Sphenolithus predistentus*		45X-5-55/57	303.95	26.93
BO *Sphenolithus ciperoensis*		45X-6-55/57	307.56	27.14
TO *Sphenolithus pseudoradians*		45X-6-105/107	310.56	28.73
BO *Sphenolithus distentus*		46X-2-55/57	314.15	30
TO *Reticulofenestra umbilicus* (>14 μm)-low latitude		49X-1-55/57	341.35	32.02
TO *Ericsonia formosus*		50X-5-55/56	356.99	32.92
Bc *Clausicoccus subdistichus*		52X-3-55/56	373.18	33.88
TO *Sphenolithus predistentus*	U1505	57X-6-1/2	407.455	26.93
TO *Reticulofenestra umbilicus* (>14 μm)-low latitude		59X-CC	424.92	32.02
Bc *Clausicoccus subdistichus*		61X-1-145/147	443.45	33.88
TO *Sphenolithus distentus*	LW22	2	3 273	26.84
TO *Sphenolithus predistentus*		3	3 285	26.93
TO *Sphenolithus pseudoradians*		13	3 395	28.73
BO *Sphenolithus distentus*		21	3 475	30
TO *Reticulofenestra umbilicus* (>14 μm)-low latitude		49	3 773	32.02
TO *Ericsonia formosus*		56	3 835	32.92

that smaller than five micrometers were all counted and calculated as the informal group small *Reticulofenestra* sp. Their relative abundances are plotted against sample number sequence from ~27 Ma to 34 Ma (Fig. 3). Nannofossils in U1505 were very rare in ~27–29 Ma, thus this part of assemblages is not included to avoid the invalidity in biometric analysis.

Total absolute abundances of nannofossils at IODP Sites U1501, U1505 and LW2 are of the same order of magnitude, and do not show any significant trend in the Early Oligocene. In our study interval, the size of nannofossils in the study interval does not change much, eliminating the possible effect of mass variation. Those taxa that are larger than ten micrometers, such as *R. umbilicus* (>14 μm), *Discoaster* spp., *Helicosphaera* spp., and *Cy. abisectus* were in low abundance, while small *Reticulofenestra* (<5 μm) are generally evenly distributed throughout our study interval (Fig. 3). Therefore, the abundance of nannofossil can to some degree be considered as the carbonate volume produced by coccolithophore. The abundance of nannofossil dramatically dropped at 32 Ma, while the nutrient proxy is at its highest value. The abundance of nannofossil soon rebounded to a higher level at about 10^9 g^{-1} in the sediment, corresponded to an increase in $CaCO_3$ content.

Assemblage compositions show a great consistent among the three study sites. It is shown that the *Cyclicargolithus* (*Cy. floridanus* and *Cy. abisectus*) was the most common and dominating taxa presented in the study interval, with a relative abundance ranging from 20% to 60%. The *Cyclicargolithus* spp. progressively increased from ~32 Ma to 31 Ma, coinciding with the decrease in relative abundance of eutrophic taxa. This represents an essential change in nannofossil assemblage. Lower photic zone genus *Discoaster* spp. and *Sphenolithus* spp. were rare and slightly increased through the studied interval, ranging from 0% to ~10%. Other species including *Pontosphaera* spp., *Braarudosphaera* spp. and *Zygbijugatus* spp. were very rare and assumed to be not important to this research (Fig. 3).

Differences of the nannoplankton community among the study sites are also documented. Several bloom-like events in the group of *R. lockeri* are found from around 34 Ma to 31 Ma, in U1501, instead the small *Reticulofenestra* were rare in this interval. *Reticulofenestra bisecta* group were more abundant during around 32–31 Ma in Site U1505, which cannot be seen in U1501 and LW2. These differences between U1501 and the other two sites may be caused by the differences in sample preservation and the sag-specific features of the seawater.

Remarkably, the E^* ratios show a great consistent trend from the three study sites. In order to compare the assemblage changes with the environmental parameters, we plotted phosphorus content in bulk sediment against the E^* ratio based on Site U1501 (Fig. 4). Among the 67 samples in IODP Site U1501, 44 samples are selected to conduct the bulk elemental analysis. The E^* ratio in these samples range from 13.82% to 68.75% (average= 40.41%). The phosphorus content varied from 60.1×10^{-6} to 351.6×10^{-6} (average=204.4×10^{-6}). The absolute values of both E^* and phosphorus content are higher in ~32.3–33.9 Ma than that in 26.9–32.3 Ma. Intriguingly, inversed patterns of correlation between E^* and bulk phosphorus content are observed. Before 32.3 Ma, the E^* ratio increased with the decreasing phosphorus (r=0.51, Fig. 4b), but the p value reaches 0.067 (>0.05), indicating a weak correlation. On the contrary, E^* is positively correlated to phosphorus changes after 32.3 Ma (r=0.56, p=0.001, Fig. 4a).

3.3 *Bulk elemental analysis*

Geochemical proxies are shown in Fig. 5. The TiO_2/Al_2O_3 ratio decreased distinctly from 3.2 to 2.4 during the period from 32 Ma to ~30.5 Ma, reaches the lowest value of 2.37 at around 31.5 Ma (Fig. 5). The K/Al ranges from around 0.19 to 0.26 with a continuous increasing trend at the whole study interval. Two shift of K/Al ratio observed at around 32 Ma and 30.5 Ma. Meanwhile the Mn/Al ratio was exclusively at low values (no larger than 0.2) during this period. The phosphorus generally decreased with little variation at around 32 Ma. The calcium carbonates increased since 30.5 Ma, and then reached its highest value of ~30% at ~29.5 Ma. The geochemical proxies were compared with the pollen analysis by Wu et al. (2003), which indicates a shift of dominating type of the terrestrial vegetation from tropical-subtropical humid taxa into temperate montane taxa.

4 Discussion

This study, based on the newly formed SCS basin in the Early Oligocene, aims to tackle the question of entangled controls of nutrient and CO_2 on the coccolithophores. The environmental controls on the fossil records are far more complex to be cap-

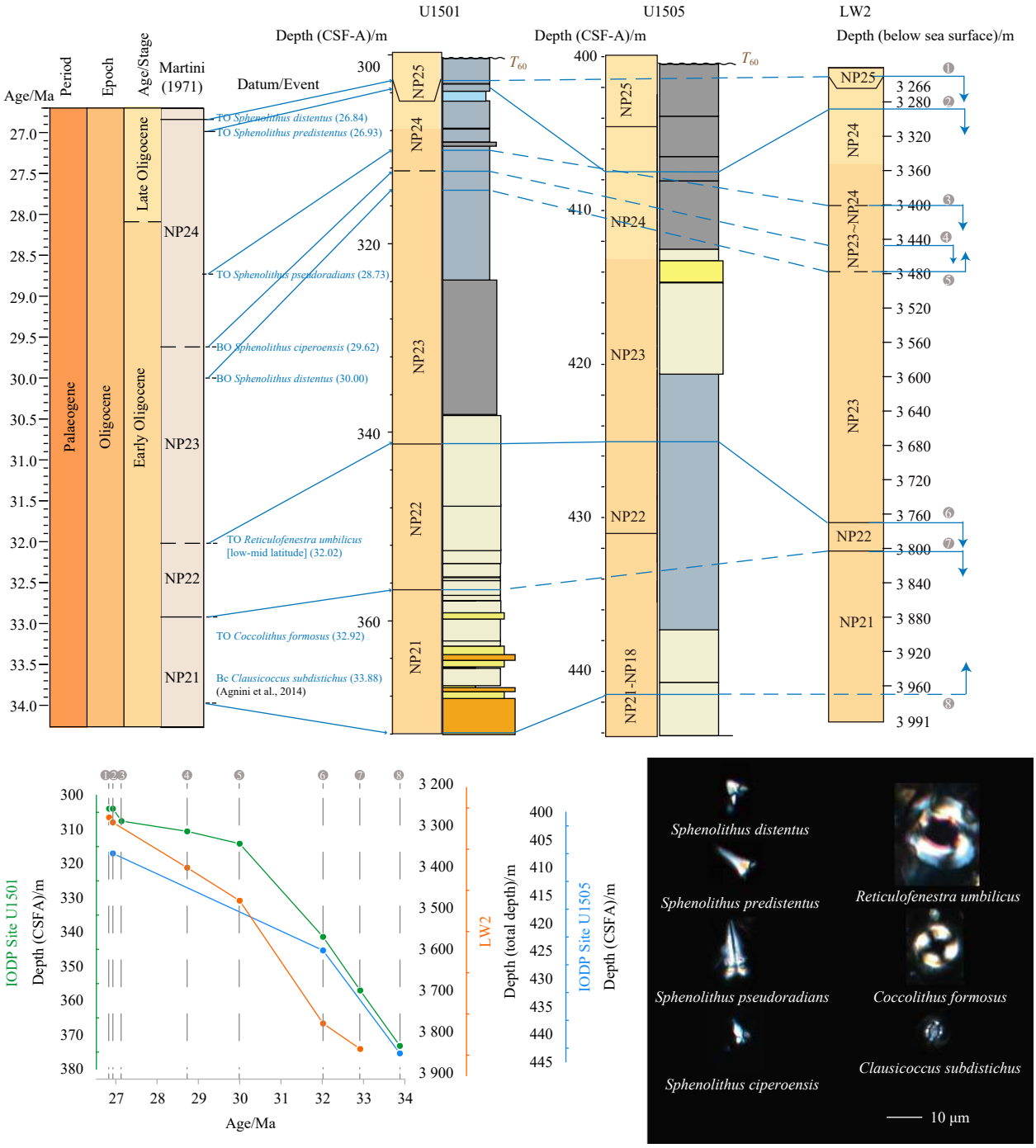

Fig. 2. Biostratigraphy for Sites U1501, U1505 and LW2 following the standard NP biozonation (Martini, 1971). Lithology study are imitated from Jian et al. (2018). Age model is established based on controlling points with a liner interpolation in between.

tured than culturing studies. Nevertheless, with rapid changes in nutrient condition (Ma et al., 2019) and CO_2 concentration (Zhang et al., 2013; Pagani et al., 2011), the northern SCS may provide an ideal natural laboratory to compare different influencing factors on the nannoplankton.

4.1 *Early Oligocene paleoenvironmental changes in the northern SCS*

East Asian Paleogene climates have long been regarded as controlled by the planetary wind system, which results in a climate pattern with three latitudinally distributed zones. Two humid zones located separately in the North China and South China were lithologically designated by coals and oil shales, while an arid zone in the middle was represented by red beds and evaporates (Liu et al., 2015; Quan et al., 2014). The paleobotanical pattern in the southern China also indicates a humid climate during the Eocene-Early Oligocene (Sun and Wang, 2005). Pollen analysis revealed that a relatively cool and arid climate had developed since 32 Ma in the neighboring continent of the northern SCS (Wu et al., 2003). This humid to arid alteration is supported by our multi-proxy analysis (Fig. 5). Decreased TiO_2/Al_2O_3 ratio revealed a lowered fluvial runoff in ~32–30.5 Ma,

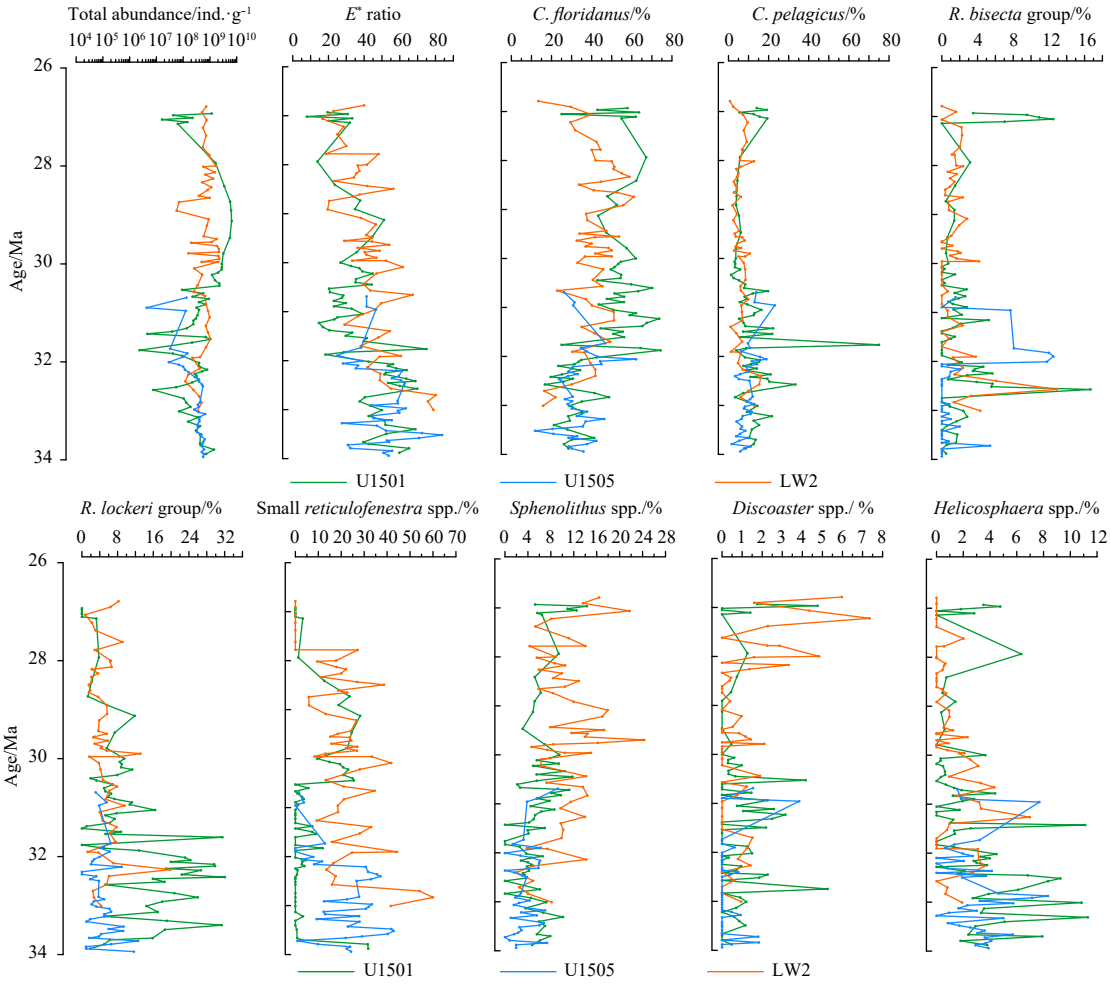

Fig. 3. Nannofossil total abundance (ind./g) in sediment, E^* ratio and taxa relative abundances in percentage. Three sites are posted in different colors.

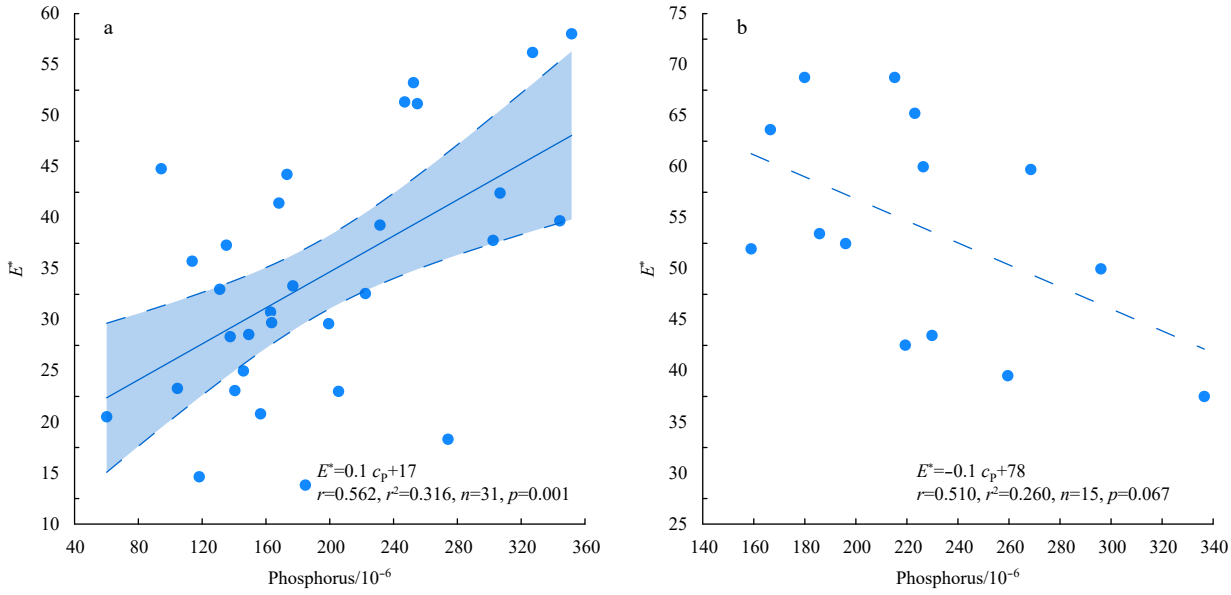

Fig. 4. Relationships of E^* ratio and bulk phosphorus content (c_P) are shown in plot graphs based on IODP Site U1501. Date from study interval of ~26.9–32.3 Ma (a) and ~32.3–33.88 Ma (b) are shown in separate, and 95% confidence intervals are shaded in blue in the left graph.

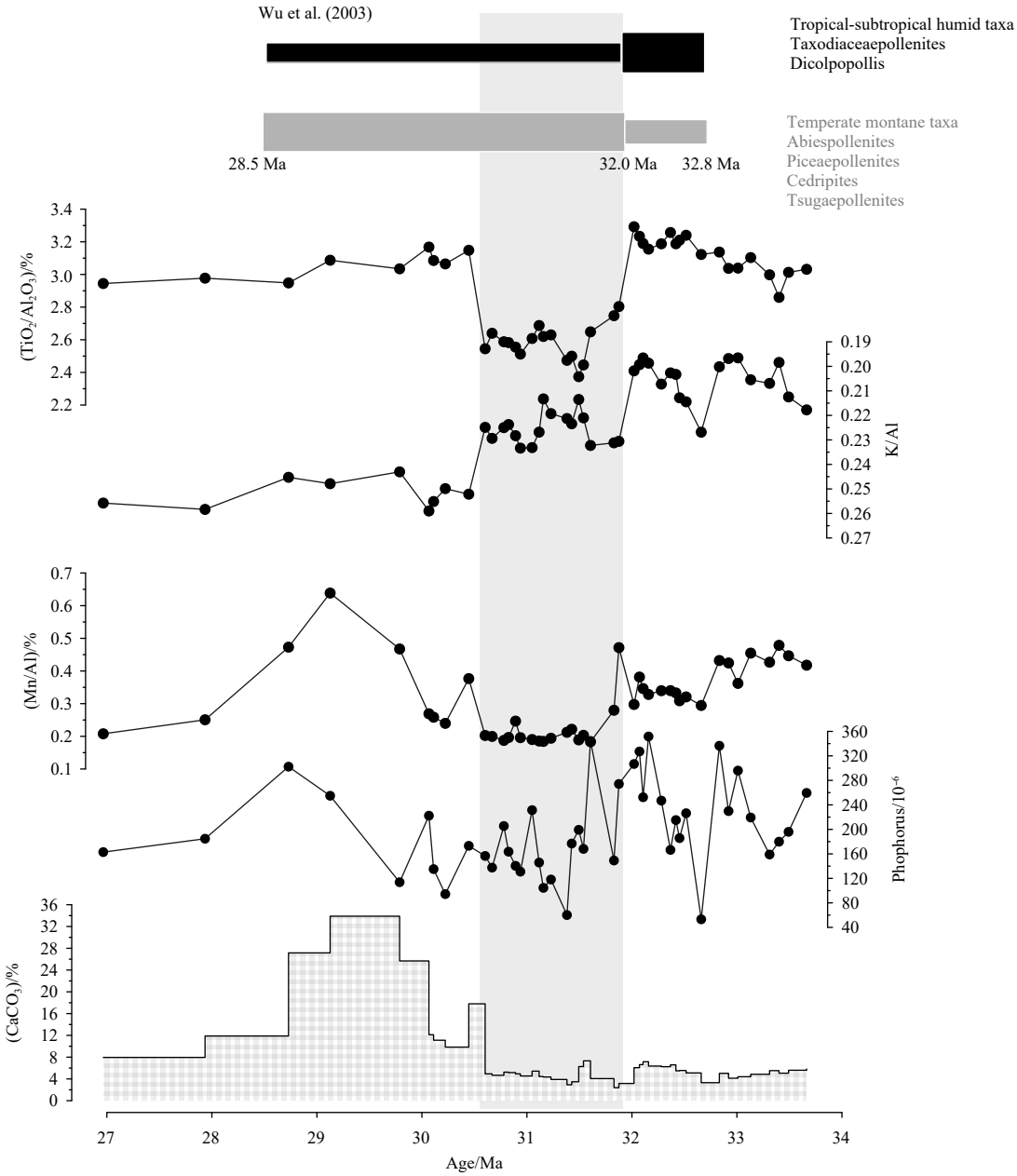

Fig. 5. Geochemical proxy records from U1501 during ~34-27 Ma. Pollen analysis from Wu et al. (2003) indicates that the Temperate Montane Taxa (black rectangle) remarkably increased since 32 Ma, whereas the taxa reflecting tropical-subtropical warm and humid climate (gray rectangle) decreased distinctly afterward.

corresponding to the reduced chemical weathering reflected by the increase in K/Al ratio. Minimum values of Mn/Al ratio during ~32–30.5 Ma suggested the anoxic bottom water, which was probably caused weak fluvial input. Together, these suggest a climate condition of low precipitation and low chemical weathering. The reduced terrestrial input ultimately results in a lower nutrient availability to nanoplanktons in the surface water, revealed by our phosphorus content in bulk sediment (Fig. 5).

Admittedly, the variations of chemical records can also be interpreted as tectonic changes. The northern SCS was attributed to a shallow-coastal environment with the seafloor progressively spreading after the rifting since ~34 Ma (Larsen et al., 2018; Li et al., 2006). The continuous geophysical parameters and sedimentary profiles show no evidence for a large tectonic event at 32 Ma (Jian et al., 2018; Larsen et al., 2018). Therefore, we eliminate the possible effect of tectonic changes and suggest that the climate pattern was changing in response to global atmospheric forces.

The declining atmospheric CO_2 was the most striking feature of climate change during this interval. The modelling studies suggest that declined CO_2 may have great influence on local environment by weakening the annual precipitation, and further induce aridity in the East Asia with decreased pressure gradient from continent to ocean (Cherchi et al., 2011; Huber and Goldner, 2012; Licht et al., 2014). Some researchers stated that the decline in global atmospheric CO_2 was resulted from increased chemical weathering of exposed silica (Gaillardet et al., 1999; Wan et al., 2017). However, no distinct sea-level decline was found during this interval, arguing against the prerequisite of enhanced chem-

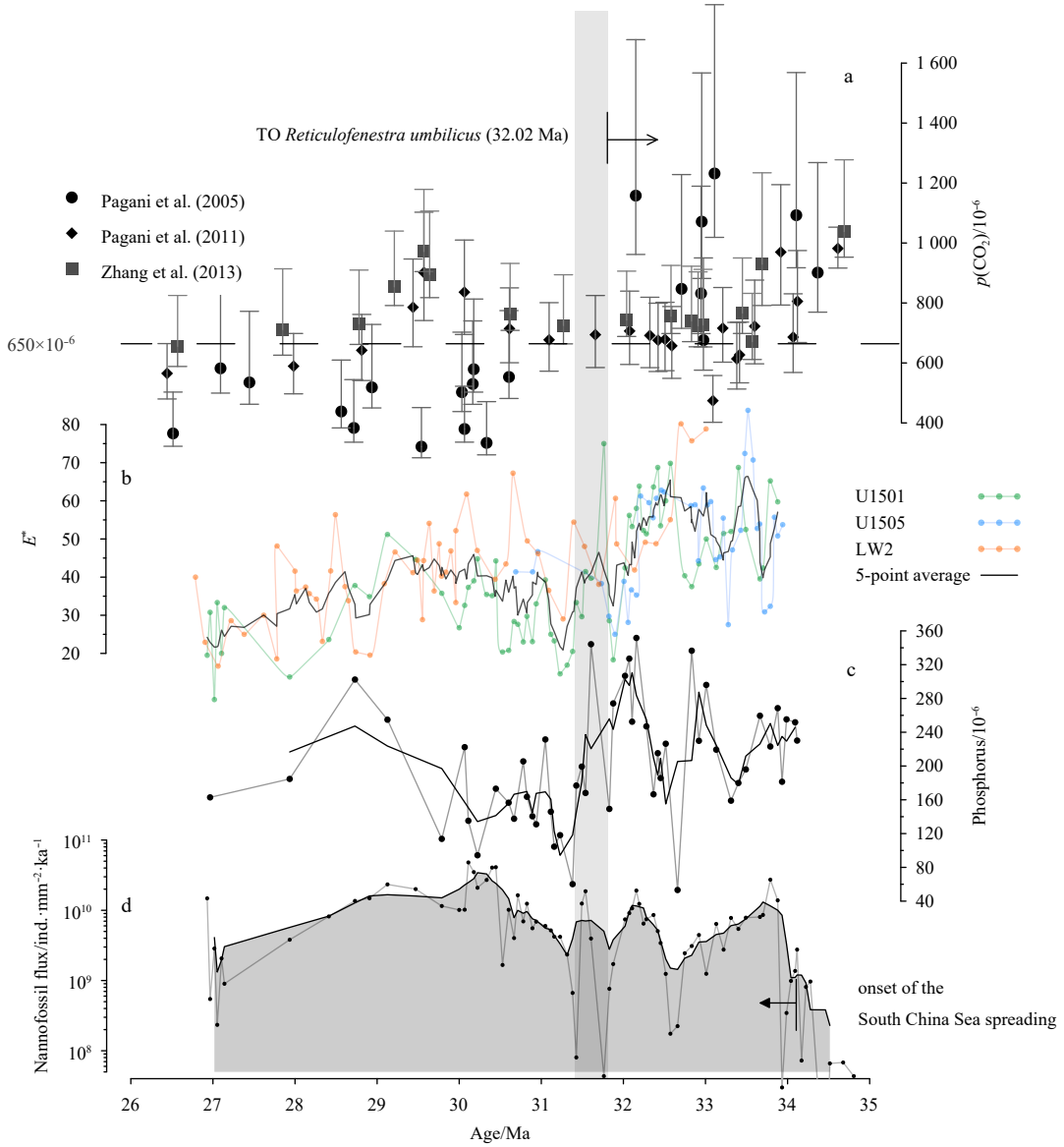

Fig. 6. Nannofossil changes related to CO_2 and nutrient. a. Accessible reconstructed CO_2 data for the study interval are cited. b. The E^* ratios of three study sites, composed curve running a 5-point average is shown in black bold. c. Phosphorus content in the bulk sediment given in $\times 10^{-6}$. d. The total abundance of Calcareous nannofossil sharply decreased but soon rebounded after 32 Ma. The dashed line marks the bio-limiting threshold 650×10^{-6} (volume fraction), calculated by function of SST for aqueous [CO_2] scenario of 19 μmol/L (the upper limits of the proposed [CO_2] threshold for the appearance of coccolith vital effects) at constant alkalinity of 2 320 μmol/L from Bolton et al. (2013). The tropical SST was adopted from Liu et al. (2009) as around 24°C. The 32 Ma is marked by the red dashed line, before and after this time, and the E^* ratio has different relation with CO_2 and phosphorus. Bio-marker TO *Reticulofenestra umbilicus* was recognized convincingly because of its outstandingly large size (>14 μm) relative to other taxa in the study interval.

ical weathering (Haq and Lohmann, 1976; Li et al., 2006).

4.2 *Nannofossil assembalge changes related to CO_2 and nutrient supply*

In our research, we test the effect of nutrient and CO_2 on the coccolithophores during the Early Oligocene, northern SCS, where both the influencing factors fluctuated in a significant magnitude. Müller et al. (2017) have shown that for the modern species *Emiliania huxleyi*, phosphate nutrient limitation caused a decrease in both photosynthesis and calcification at all CO_2 levels (ranges from 0 to 2 000 μatm, 1 atm=101.325 kPa). However, the response to phosphate is less sensitive under a nutrient-replete condition. In this case, nutrient controls the cell's growth under oligotrophic conditions. Once nutrient became replete, there will be no more promotive effects but only constraint of CO_2 concentration. This scenario was further supported by culturing studies by Bach et al. (2015).

During the Eocene-Oligocene climate transition, nannofossil assemblage study is an indispensable way to peer into the physiologic characteristics. A prolonged influence has caved in the structure of the coccolith, revealed by the decrease of the species with robust skeleton structure, suggesting that the Eocene/Oligocene event had a marked filter effect on Eocene nanoplanktons (Aubry and Bord, 2009). Instead of nutrient limitation, Hen-

deriks and Pagani (2008) attribute the variation of coccolith size to CO_2 changes. The CO_2 decline makes it more difficult for larger cells to acquire enough CO_2 due to their relatively lower surface area/volume ratio. In order to acquire more carbon sources from the seawater, previous studies have suggested that coccolithophore might initiate CCM in the low CO_2 condition (Bach et al., 2013; Badger et al., 1998; Bolton and Stoll, 2013; Reinfelder, 2011; Riebesell, 2004; Rost et al., 2003). We tentatively adopt 19 μmol/L as the upper limit of CCM initiating threshold from culturing research (Bolton and Stoll, 2013). With reconstructed Early Oligocene tropical Pacific sea surface temperature of ~25°C (Liu et al., 2009), the estimated $p(CO_2)$ is around 650×10^{-6} (volume fraction) (dashed horizontal line in Fig. 6a). The CO_2 concentration reached to this value in the Early Oligocene (Fig. 6). Comparing with our assemblage data, we suggest the changes in nannofossil were triggered by the carbonate chemistry condition in the ocean. With the continuous decrease in atmospheric CO_2 from the Eocene, weakened diffusive efficiency had caused a great limitation of carbon sources for coccolithophores. When CO_2 distinctly declined after 32 Ma, the E^* ratio changed synchronously with nutrient supply. This tendency can, to some degree, indicate that coccolithophore was more sensitive to CO_2 when the CCM has not progressed. When the $p(CO_2)$ declined to lower than $\sim650\times10^{-6}$ (volume fraction) since 32 Ma, the E^* ratio is more correlated with phosphorus. In this scenario, we infer that the CCM guarantees the carbon source for both calcification and photosynthesis, making nutrient the most limiting factor. Our results further imply that long-term coccolithophore species shifts as a result of oceanic changes will potentially have a more significant impact on carbon cycle feedbacks in the future, highlighting the importance of studying integrated community calcification.

5 Conclusions

In this study, as revealed by geochemical records, a decreased weathering intensity, which reinforced the relatively arid changing event was found in the northern SCS since 32 Ma. Nannofossil assemblage index, E^* ratio, is introduced. The index comprised of relative abundance between eutrophic and mesooligotrophic taxa shows a great correlation with bulk phosphorous content with opposite covary patterns at different time intervals. Relatively weaker nutrient limitation is found under the higher CO_2 condition, while nutrient limitation strengthened under the lower CO_2 condition. We suggest that with CO_2 concentration above the threshold value, the assemblage changes were strongly influenced by the carbon source. After the great decline of CO_2, our data suggest that nutrient availability tends to be the most limiting factor of coccolithophores growth. By comparing with Bolton and Stoll (2013) threshold value (650×10^{-6}, volume fraction), we infer that the initiation of the CCM might have strengthened the uptake of carbon sources from the seawater.

Admittedly, the lightness and salinity are two other possible influencing factors that are very difficult to reconstruct and have not been discussed in this study. Furthermore, it also lacks precise calculation to draw a conclusion only by nannofossil abundance, as the mass, volume, and growth rate of coccolith also matter to the production of biogenic carbonate. The relationship between coccolithophore and the global carbon cycle is yet to be revealed by quantitative studies in the future.

Acknowledgements

Samples and data used in this research were provided by the International Ocean Discovery Program (IODP). We are grateful to all the shipboard scientists of IODP Expedition 367/368. Geochemical measurements were performed in the State Key Laboratory of Marine Geology, Tongji University, under the supervision of Peijun Qiao. Xiaobo Jin acknowledge the National Natural Science Foundation of China under contract No. 41806050. In the end, this study would not have been possible without the help of M-P Aubry on Paleogene calcareous nannofossil taxonomy.

References

Aubry M P. 1992. Paleogene calcareous nannofossils from the Kerguelen Plateau, Leg 120. In: Wise S, Schlich R, eds. Proceedings of the Ocean Drilling Program, Scientific Results, 120: 471–491

Aubry M P. 2007. A major Pliocene coccolithophore turnover: Change in morphological strategy in the photic zone. In: Monechi S, Coccioni R, Rampino M, eds. Large Ecosystem Perturbations: Causes and Consequences. The Geological Society of America, Special Paper, 424: 25–51

Aubry M P. 2009. A sea of Lilliputians. Palaeogeography, Palaeoclimatology, Palaeoecology, 284(1–2): 88–113, doi: 10.1016/j.palaeo.2009.08.020

Aubry M P, Bord D. 2009. Reshuffling the cards in the photic zone at the Eocene/Oligocene boundary. In: Koeberl C, Montanari A, eds. The Late Eocene Earth: Hothouse, Icehouse, and Impacts. The Geological Society of America, Special Paper, 452: 279–301

Auer G, Piller W E, Harzhauser M. 2014. High-resolution calcareous nannoplankton palaeoecology as a proxy for small-scale environmental changes in the Early Miocene. Marine Micropaleontology, 111: 53–65, doi: 10.1016/j.marmicro.2014.06.005

Bach L T, Mackinder L C M, Schulz K G, et al. 2013. Dissecting the impact of CO_2 and pH on the mechanisms of photosynthesis and calcification in the coccolithophore *Emiliania huxleyi*. New Phytologist, 199(1): 121–134, doi: 10.1111/nph.12225

Bach L T, Riebesell U, Gutowska M A, et al. 2015. A unifying concept of coccolithophore sensitivity to changing carbonate chemistry embedded in an ecological framework. Progress in Oceanography, 135: 125–138, doi: 10.1016/j.pocean.2015.04.012

Badger M R, Andrews T J, Whitney S M, et al. 1998. The diversity and coevolution of Rubisco, plastids, pyrenoids, and chloroplast-based CO_2-concentrating mechanisms in algae. Canadian Journal of Botany, 76(6): 1052–1071, doi: 10.1139/b98-074

Bolton C T, Stoll H M. 2013. Late Miocene threshold response of marine algae to carbon dioxide limitation. Nature, 500(7464): 558–562, doi: 10.1038/nature12448

Bordiga M, Bartol M, Henderiks J. 2015. Absolute nannofossil abundance estimates: Quantifying the pros and cons of different techniques. Revue de Micropaléontologie, 58(3): 155–165, doi: 10.1016/j.revmic.2015.05.002

Bown P R, Lees J A, Young J R. 2004. Calcareous nannoplankton evolution and diversity through time. In: Thierstein H R, Young J R, eds. Coccolithophores. Berlin, Heidelberg: Springer, 481–508

Cachão M, Moita M T. 2000. *Coccolithus pelagicus*, a productivity proxy related to moderate fronts off Western Iberia. Marine Micropaleontology, 39(1–4): 131–155, doi: 10.1016/S0377-8398(00)00018-9

Calvert S E, Pedersen T F. 2007. Chapter fourteen elemental proxies for palaeoclimatic and palaeoceanographic variability in marine sediments: Interpretation and application. Developments in Marine Geology, 1: 567–644, doi: 10.1016/S1572-5480(07)01019-6

Cherchi A, Alessandri A, Masina S, et al. 2011. Effects of increased CO_2 levels on monsoons. Climate Dynamics, 37(1–2): 83–101, doi: 10.1007/s00382-010-0801-7

Clift P D, Wan Shiming, Blusztajn J. 2014. Reconstructing chemical weathering, physical erosion and monsoon intensity since 25Ma in the northern South China Sea: A review of competing proxies. Earth-Science Reviews, 130: 86–102, doi: 10.1016/j.earscirev.2014.01.002

Cramer B S, Miller K G, Barrett P J, et al. 2011. Late Cretaceous-Neo-

gene trends in deep ocean temperature and continental ice volume: Reconciling records of benthic foraminiferal geochemistry ($\delta^{18}O$ and Mg/Ca) with sea level history. Journal of Geophysical Research, 116(C12): C12023, doi: 10.1029/2011JC007255

Cramer B S, Toggweiler J R, Wright J D, et al. 2009. Ocean overturning since the Late Cretaceous: Inferences from a new benthic foraminiferal isotope compilation. Paleoceanography, 24(4): PA4216

Dunkley Jones T, Bown P R, Pearson P N, et al. 2008. Major shifts in calcareous phytoplankton assemblages through the Eocene-Oligocene transition of Tanzania and their implications for low-latitude primary production. Paleoceanography, 23(4): PA4204

Feng Yuanyuan, Roleda M Y, Armstrong E, et al. 2017. Environmental controls on the growth, photosynthetic and calcification rates of a Southern Hemisphere strain of the coccolithophore *Emiliania huxleyi*. Limnology and Oceanography, 62(2): 519–540, doi: 10.1002/lno.10442

Filippelli G M. 2002. The global phosphorus cycle. Reviews in Mineralogy and Geochemistry, 48(1): 391–425, doi: 10.2138/rmg.2002.48.10

Fioroni C, Villa G, Persico D, et al. 2015. Middle Eocene-Lower Oligocene calcareous nannofossil biostratigraphy and paleoceanographic implications from Site 711(equatorial Indian Ocean). Marine Micropaleontology, 118: 50–62, doi: 10.1016/j.marmicro.2015.06.001

Fernando A G S, Peleo-Alampay A M, Wiesner M G. 2007. Calcareous nannofossils in surface sediments of the eastern and western South China Sea. Marine Micropaleontology, 66(1): 1–26, doi: 10.1016/j.marmicro.2007.07.003

Flores J A, Sierro F J, Raffi I. 1995. Evolution of the calcareous nannofossil assemblage as a response to the paleoceanographic changes in the eastern equatorial Pacific Ocean from 4 to 2 Ma (Leg 138, Sites 849 and 852). In: Pisias N G, Mayer L A, Janecek T R, et al., eds. Proceedings of the Ocean Drilling Program, Scientific Results, 138: 163-176

Gaillardet J, Dupré B, Louvat P, et al. 1999. Global silicate weathering and CO_2 consumption rates deduced from the chemistry of large rivers. Chemical Geology, 159(1–4): 3–30, doi: 10.1016/S0009-2541(99)00031-5

Haq B U, Lohmann G P. 1976. Early Cenozoic calcareous nannoplankton biogeography of the Atlantic Ocean. Marine Micropaleontology, 1: 119–194, doi: 10.1016/0377-8398(76)90008-6

Henderiks J, Pagani M. 2008. Coccolithophore cell size and the Paleogene decline in atmospheric CO_2. Earth and Planetary Science Letters, 269(3–4): 576–584, doi: 10.1016/j.epsl.2008.03.016

Huber M, Goldner A. 2012. Eocene monsoons. Journal of Asian Earth Sciences, 44: 3–23, doi: 10.1016/j.jseaes.2011.09.014

Jatiningrum R S, Sato T. 2017. Sea-surface dynamics changes in the Subpolar North Atlantic Ocean (IODP Site U1314) during Late Pliocene climate transition based on calcareous Nannofossil observation. Open Journal of Geology, 7(10): 1538–1551, doi: 10.4236/ojg.2017.710103

Jian Zhimin, Larsen H C, Alvarez Zarikian C A, et al. 2018. Expedition 368 Preliminary Report: South China Sea Rifted Margin. Texas: International Ocean Discovery Program, 1–54

Jian Zhimin, Jin Haiyan, Kaminski M A, et al. 2019. Discovery of the marine Eocene in the northern South China Sea. National Science Review, 6(5): 881–885, doi: 10.1093/nsr/nwz084

Jin Xiaobo, Liu Chuanlian, Poulton A J, et al. 2016. Coccolithophore responses to environmental variability in the South China Sea: species composition and calcite content. Biogeosciences, 13(16): 4843–4861, doi: 10.5194/bg-13-4843-2016

Koch C, Young J R. 2007. A simple weighing and dilution technique for determining absolute abundances of coccoliths from sediment samples. Journal of Nannoplankton Research, 29(1): 67–69

Krumhardt K M, Lovenduski N S, Iglesias-Rodriguez M D, et al. 2017. Coccolithophore growth and calcification in a changing ocean. Progress in Oceanography, 159: 276–295, doi: 10.1016/j.pocean.2017.10.007

Larsen H C, Mohn G, Nirrengarten M, et al. 2018. Rapid transition from continental breakup to igneous oceanic crust in the South China Sea. Nature Geoscience, 11(10): 782–789, doi: 10.1038/s41561-018-0198-1

Li Qianyu, Wang Pinxian, Zhao Quanhong, et al. 2006. A 33 Ma lithostratigraphic record of tectonic and paleoceanographic evolution of the South China Sea. Marine Geology, 230(3–4): 217–235, doi: 10.1016/j.margeo.2006.05.006

Licht A, van Cappelle M, Abels H A, et al. 2014. Asian monsoons in a late Eocene greenhouse world. Nature, 513(7519): 501–506, doi: 10.1038/nature13704

Liu Xiaodong, Guo Qingchun, Guo Zhengtang, et al. 2015. Where were the monsoon regions and arid zones in Asia prior to the Tibetan Plateau uplift?. National Science Review, 2(4): 403–416, doi: 10.1093/nsr/nwv068

Liu Zhonghui, Pagani M, Zinniker D, et al. 2009. Global cooling during the eocene-oligocene climate transition. Science, 323(5918): 1187–1190, doi: 10.1126/science.1166368

Ma Ruigang, Liu Chuanlian, Li Qianyu, et al. 2019. Calcareous nannofossil changes in response to the spreading of the South China Sea basin during Eocene-Oligocene. Journal of Asian Earth Sciences, 184: 103963, doi: 10.1016/j.jseaes.2019.103963

Martini E. 1971. Standard Tertiary and Quaternary calcareous nannoplankton zonation. In: Farinacci A, ed. Proceedings of the 2nd Planktonic Conference, Roma. Tecnoscienza, 2: 739–785

McKay C L, Groeneveld J, Filipsson H L, et al. 2015. A comparison of benthic foraminiferal Mn/Ca and sedimentary Mn/Al as proxies of relative bottom-water oxygenation in the low-latitude NE Atlantic upwelling system. Biogeosciences, 12(18): 5415–5428, doi: 10.5194/bg-12-5415-2015

Müller M N, Antia A N, LaRoche J. 2008. Influence of cell cycle phase on calcification in the coccolithophore *Emiliania huxleyi*. Limnology and Oceanography, 53(2): 506–512, doi: 10.4319/lo.2008.53.2.0506

Müller M, Trull T W, Hallegraeff G M. 2017. Independence of nutrient limitation and carbon dioxide impacts on the Southern Ocean coccolithophore *Emiliania huxleyi*. The ISME Journal, 11(8): 1777–1787, doi: 10.1038/ismej.2017.53

Neretin L N, Pohl C, Jost G, et al. 2003. Manganese cycling in the Gotland Deep, Baltic Sea. Marine Chemistry, 82(3–4): 125–143, doi: 10.1016/S0304-4203(03)00048-3

Newsam C, Bown P R, Wade B S, et al. 2017. Muted calcareous nannoplankton response at the Middle/Late Eocene Turnover event in the western North Atlantic Ocean. Newsletters on Stratigraphy, 50(3): 297–309, doi: 10.1127/nos/2016/0306

Pagani M, Huber M, Liu Zhonghui, et al. 2011. The role of carbon dioxide during the onset of Antarctic glaciation. Science, 334(6060): 1261–1264, doi: 10.1126/science.1203909

Pagani M, Zachos J C, Freeman K H, et al. 2005. Marked decline in atmospheric carbon dioxide concentrations during the Paleogene. Science, 309(5734): 600–603, doi: 10.1126/science.1110063

Perrin L, Probert I, Langer G, et al. 2016. Growth of the coccolithophore *Emiliania huxleyi* in light- and nutrient-limited batch reactors: relevance for the BIOSOPE deep ecological niche of coccolithophores. Biogeosciences, 13(21): 5983–6001, doi: 10.5194/bg-13-5983-2016

Persico D, Villa G. 2004. Eocene-Oligocene calcareous nannofossils from Maud Rise and Kerguelen Plateau (Antarctica): paleoecological and paleoceanographic implications. Marine Micropaleontology, 52(1–4): 153–179, doi: 10.1016/j.marmicro.2004.05.002

Plancq J, Mattioli E, Henderiks J, et al. 2013. Global shifts in Noelaerhabdaceae assemblages during the late Oligocene-early Miocene. Marine Micropaleontology, 103: 40–50, doi: 10.1016/j.marmicro.2013.07.004

Poulton A J, Adey T R, Balch W M, et al. 2007. Relating coccolithophore calcification rates to phytoplankton community dynamics: Regional differences and implications for carbon export. Deep Sea Research Part II: Topical Studies in Oceanography, 54(5–7): 538–557, doi: 10.1016/j.dsr2.2006.12.003

Quan Cheng, Liu Zhonghui, Utescher T, et al. 2014. Revisiting the Paleogene climate pattern of East Asia: A synthetic review. Earth-Science Reviews, 139: 213–230, doi: 10.1016/j.earscirev.2014.09.005

Raffi I, Agnini C, Backman J, et al. 2016. A Cenozoic calcareous nannofossil biozonation from low and middle latitudes: a synthesis. Journal of Nannoplankton Research, 36(2): 121–132

Reinfelder J R. 2011. Carbon concentrating mechanisms in eukaryotic marine phytoplankton. Annual Review of Marine Science, 3: 291–315, doi: 10.1146/annurev-marine-120709-142720

Riebesell U. 2004. Effects of CO_2 enrichment on marine phytoplankton. Journal of Oceanography, 60(4): 719–729, doi: 10.1007/s10872-004-5764-z

Rost B, Riebesell U, Burkhardt S, et al. 2003. Carbon acquisition of bloom-forming marine phytoplankton. Limnology and Oceanography, 48(1): 55–67, doi: 10.4319/lo.2003.48.1.0055

Schmitz B. 1987. The TiO_2/Al_2O_3 ratio in the Cenozoic Bengal Abyssal Fan sediments and its use as a paleostream energy indicator. Marine Geology, 76: 195–206, doi: 10.1016/0025-3227(87)90029-6

Shimmield G B, Mowbray S R. 1991. The inorganic geochemical record of the northwest Arabian Sea: A history of productivity variation over the last 400 ky from site 722 and 724. In: Prell W, Niitsuma, eds. Proceedings of Ocean Drilling Program, Scientific Results, 117: 409–429

Sun Xiangjun, Wang Pinxian. 2005. How old is the Asian monsoon system?—Palaeobotanical records from China. Palaeogeography, Palaeoclimatology, Palaeoecology, 222(3–4): 181–222, doi: 10.1016/j.palaeo.2005.03.005

Tangunan D N, Baumann K H, Just J, et al. 2018. The last 1 million years of the extinct genus *Discoaster*: Plio-Pleistocene environment and productivity at Site U1476(Mozambique Channel). Palaeogeography, Palaeoclimatology, Palaeoecology, 505: 187–197, doi: 10.1016/j.palaeo.2018.05.043

Toffanin F, Agnini C, Fornaciari E, et al. 2011. Changes in calcareous nannofossil assemblages during the Middle Eocene Climatic Optimum: Clues from the central-western Tethys (Alano section, NE Italy). Marine Micropaleontology, 81(1–2): 22–31, doi: 10.1016/j.marmicro.2011.07.002

Tribovillard N, Algeo T J, Lyons T, et al. 2006. Trace metals as paleoredox and paleoproductivity proxies: An update. Chemical Geology, 232(1–2): 12–32, doi: 10.1016/j.chemgeo.2006.02.012

Villa G, Fioroni C, Pea L, et al. 2008. Middle Eocene-late Oligocene climate variability: Calcareous nannofossil response at Kerguelen Plateau, Site 748. Marine Micropaleontology, 69(2): 173–192, doi: 10.1016/j.marmicro.2008.07.006

Wan Shiming, Clift P D, Zhao Debo, et al. 2017. Enhanced silicate weathering of tropical shelf sediments exposed during glacial lowstands: A sink for atmospheric CO_2. Geochimica et Cosmochimica Acta, 200: 123–144, doi: 10.1016/j.gca.2016.12.010

Wang Pinxian. 1999. Response of Western Pacific marginal seas to glacial cycles: Paleoceanographic and sedimentological feature. Marine Geology, 156(1–4): 5–39, doi: 10.1016/S0025-3227(98)00172-8

Wu Jiawang, Böning P, Pahnke K, et al. 2016. Unraveling North-African riverine and eolian contributions to central Mediterranean sediments during Holocene sapropel S1 formation. Quaternary Science Reviews, 152: 31–48, doi: 10.1016/j.quascirev.2016.09.029

Wu Guoxuan, Qin Jungan, Mao Shaozhi. 2003. Deep-water Oligocene pollen record from South China Sea. Chinese Science Bulletin, 48(22): 2511–2515

Young J R, Bown P R, Lees J A. 2018. Nannotax3. International Nannoplankton Association. http://ina.tmsoc.org/Nannotax3 [2007-01-01/2019-01-01]

Zachos J, Pagani M, Sloan L, et al. 2001. Trends, rhythms, and aberrations in global climate 65 Ma to present. Science, 292(5517): 686–693, doi: 10.1126/science.1059412

Zhang Yige, Pagani M, Liu Zhonghui, et al. 2013. A 40-million-year history of atmospheric CO_2. Philosophical Transactions of the Royal Society A: Mathematical, Physical and Engineering Sciences, 371(2001): 20130096, doi: 10.1098/rsta.2013.0096

Zhang Gongcheng, Wang Pujun, Wu Jingfu, et al. 2015. Tectonic cycle of marginal oceanic basin: A new evolution model of the South China Sea. Earth Science Frontiers (in Chinese), 22(3): 27–37